University of Glasgow
DEPARTMENT OF
AEROSPACE
ENGINEERING

Distributed Onboard Control of a Planar Ring of Satellites

A. Gavin Y. Johnston

Department of Aerospace Engineering Report No. 9627
December 13, 1996

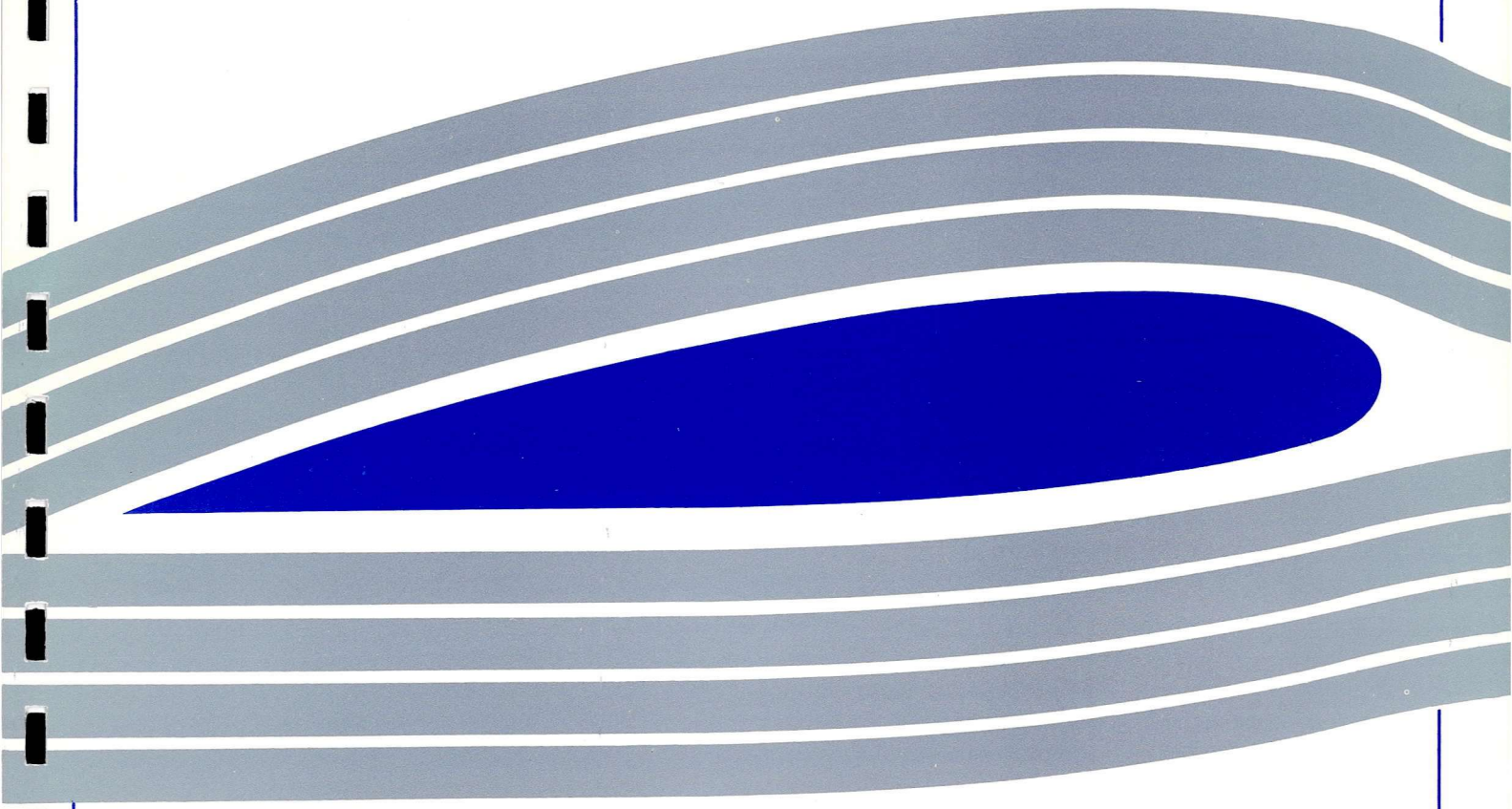

Distributed Onboard Control of a Planar Ring of Satellites

A. Gavin Y. Johnston

Department of Aerospace Engineering Report No. 9627
December 13, 1996

Department of Aerospace Engineering,
University of Glasgow
Glasgow G12 8QQ
United Kingdom

Tel. : +44 (0) 141 339–8855
FAX : +44 (0) 141 330–5560
E–mail : gjohnsto@aero.gla.ac.uk
URL : http://www.aero.gla.ac.uk

Abstract

Constellations of satellites are of growing importance in the communications and navigational fields. A number of systems ranging from a dozen satellites in high orbits to several hundred in low orbits have been proposed. Communications constellations are required to maintain certain coverage patterns, and therefore the spacing of the satellites must be tightly maintained against external perturbations such as air drag.

Controlling such systems using conventional, ground-based techniques may prove to be time-consuming and expensive, fully autonomous approaches to orbit control for satellite constellations could offer significant cost advantages. This report documents progress towards the development of control algorithms for multi-satellite constellations.

The developement of a simple, numerical Earth Satellite model is discussed, particular attention is paid to deriving a system of equations which is efficient to integrate and robust.

A control technique is developed, based on the Potential Function Method previously applied to spacecraft control problems. The resulting algorithms allow direct control of a spacecraft's orbital elements and permit exploitation of natural orbital dynamics, such as earth gravity field harmonics to adjust a spacecraft's orbit.

The application of the algorithm to maintenance of orbital altitude against air drag is successfully attempted and a distributed control scheme for a ring of satellites is developed. The distributed control is found to offer higher performance than previous techniques. Improvements to the method to avoid some unwelcome features are discussed.

Contents

List of Tables

List of Figures

Nomenclature

Notes: 1.All units SI.
2.Overlines denote reference conditions, unless otherwise stated

Roman Letters

a	Semi-Major Axis, Acceleration
b	
C_D	Drag Coefficient
e	Eccentricity
H	Scale Height
i	Inclination
J_2	(=1.023e-3)
K	Eccentric Anomaly
L	
¿	True Longitude
l	Mean Longitude
M	Mean Anomaly
m	Mass
N	Number of Satellites
n	Mean Motion
p	$a(1-e^2)$
R_e	Earth Radius
r	Orbit radius
S	Area
$s(t)$	Switching Function
t	Time
u	True Latitude
V	Speed.
v	Velocity
x, y, z	Cartesian coordinates

Greek Symbols

α	Element vector
β	Ballistic Coefficient
ϕ	Phase Angle
Φ	Potential Function
κ	Gain parameter
λ	Scaling parameter
μ	Planetary gravitational constant
ρ_0	Base Density
θ	True anomaly
ρ	Density
ϖ	Argument of Perigee measured from the node.
Ω	Right Angle of the Ascending Node
ω	Argument of perigee
τ	Time of perigee passage

Superscripts/Subscripts

a	Apogee, Semi-Major axis
$drag$	Aerodynamic Drag.
db	Deadband
$dr, d\theta, dn$	Radial, Normal and Tangential directions.
e	Eccentricity
i, j	Summation superscripts
$mean$	Mean
ref	Reference

1 Introduction

In recent years, Satellite constellations (ie arrangements of 2, or more, satellites) have been seen to offer a number of advantages for a variety of applications.[1]

- Continuous global coverage.
- Reduced system costs due to many smaller, cheaper satellites and/or smaller ground stations.
- Increased system reliability, as the system is less dependent on individual satellites.

Of particular importance to navigational and telecommunications users is the provision of continuous, global coverage, however constellations featuring large numbers of small satellites in low orbit may offer lower cost and increased overall system reliability for applications such as Earth Observation and Space Science.[2]

Research on constellations initially concentrated on finding arrangements of satellites that minimised the number of satellites required to meet certain coverage requirements. Initial work in the 1960s concentrated on circular, polar orbiting constellations requiring as few as 6 satellites for single, global coverage. These systems were, however, later found to bias coverage towards the Earth's polar regions and during the 1970s research concentrated on constellations at arbitrary inclination, with particular regard to the Global Positioning System (GPS) then under development.[3]

One of the most extensive studies of such systems was undertaken by John Walker, in the UK during the 1970s, at the then Royal Aircraft Establishment. Walker derived optimal satellites requiring as few as 5 satellites for single global coverage and laid the basis for much later work on constellation design.[4]

In recent years constellation studies have moved away from refinements in orbital geometry to detailed system studies and spacecraft design. Improvements in small spacecraft technology, undoubtedly led by the US SDI ("Star Wars") project, and expanding communications markets led to serious study of large mobile communications constellations. A number of such systems have been funded and are currently being prepared for launch within the next 5 years.[5] The characteristics of a range of proposed communications constellations are shown in Table 1.

For global coverage, satellites are usually placed into circular orbits at some common inclination (regional coverage may require elliptical orbits, but these are beyond the scope of this report). Figure 1 shows the general orbital arrangement of a typical constellation. The satellites are grouped into

into a number of distinct orbital planes, each containing an evenly distributed group of active satellites and at least 1 on-orbit spare, to provide a back-up in the event of satellite loss.

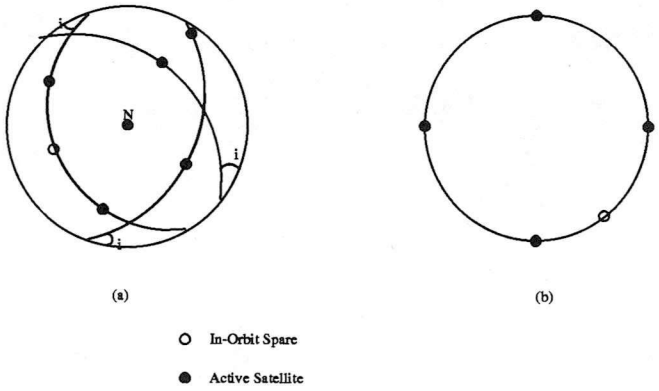

Figure 1: Orbital arrangement of constellation patterns (a) View from above pole showing 3 planes at inclination, i containing active satellites and spares. (b) View of along normal to a plane showing even spacing of active satellites and in-orbit spare.

To maintain the required coverage pattern, it will be necessary for a constellation's members to maintain their relative positions against perturbations such as differential air drag. It is evident from the data in Table 1 that this will involve controlling the orbits of dozens, or even hundreds, of satellites. As the cost and complexity of ground-based control on this scale could prove to be prohibitive, it may be advantageous to consider fully autonomous constellation control systems.

Although a considerable quantity of literature on the properties and design of constellations has been produced since the early 1960s, and interest has been shown in automating the individual satellites' onboard systems,[6,7] little appears to have been published on the problems of automating the orbit control of such systems.

Glickman[8] proposed an autonomous control scheme, which indirectly maintains even spacing by the controlling times and longitudes of equat-

Constellation	Altitude (km)	Inclination (deg)	Number of Sats
Iridium	780	86.4	66
Teledesic	695-705	98.16	840
Globalstar	1410	52	48
ICO	10355	45	12

Table 1: Characteristics of a number of proposed constellations

orial passage, of individual satellites, to pre-calculated values. However, this method is not able to directly control orbital eccentricity or reform the constellation around a failed, or newly introduced member.

A distributed scheme has been proposed by McInnes,[9] which directly controls inter-satellite spacing. In theory, this allows an evenly spaced configuration to be formed from any initial condition, without ground intervention. However, the control laws were derived assuming near-circular orbits, in practice, this assumption limits the applicability of the control to small errors in angular and radial spacing. Furthermore, the control laws derived depended on the availability of continuous, low thrust propulsion. Practical algorithms should be able to operate using small impulses.

To the author's knowledge, to date no study has successfully attempted the autonomous control of a complete 3D constellation. This study aims to demonstrate the viability of a control scheme, based on a previously presented scheme,[9] modified for use with impulsive controls. Although only control of a 2 dimensional ring of satellites will be attempted, consideration will be given to expanding the control laws to 3D cases at some later date.

The structure of this report is as follows: the equations describing the satellites' orbital evolution will be developed, paying attention to the choice of parameters to avoid singularities; the basic form of the control algorithms will be developed, and implementation as part of a satellite control system will be discussed; and finally, the control will be demonstrated for both single and multiple satellite configurations.

2 System Dynamics

2.1 Integration Scheme

The orbits of the spacecraft are modelled in the Geocentric Inertial (GCI) frame of reference. The GCI system originates at the Earth's centre of mass. The z axis points north along the Earth's polar axis, the x points in the direction of the Vernal equinox, as shown in Figure 2, the x-y plane is coplanar with the equator.

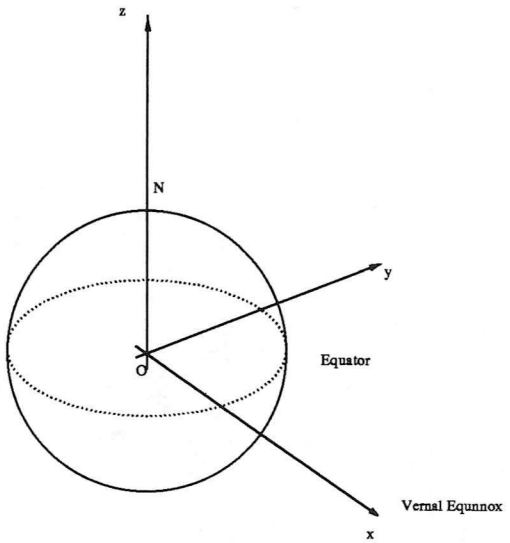

Figure 2: The GCI frame of reference

Although it is possible to integrate a spacecraft's position in terms of the cartesian coordinates $[x\ y\ z]$, it is usually more efficient to work with the 6 orbital elements. These parameters describe the size, shape and orientation of the orbit in space (see Figures 4 and 3).

In the GCI system the orbital elements are:

- Semi-Major Axis, a describing the size of the orbital ellipse.

$$a = \frac{r_a + r_p}{2} \tag{1}$$

- eccentricity, e describes how far the orbital ellipse diverges from a perfect circle

$$e = \frac{r_a - r_p}{r_a + r_p} \tag{2}$$

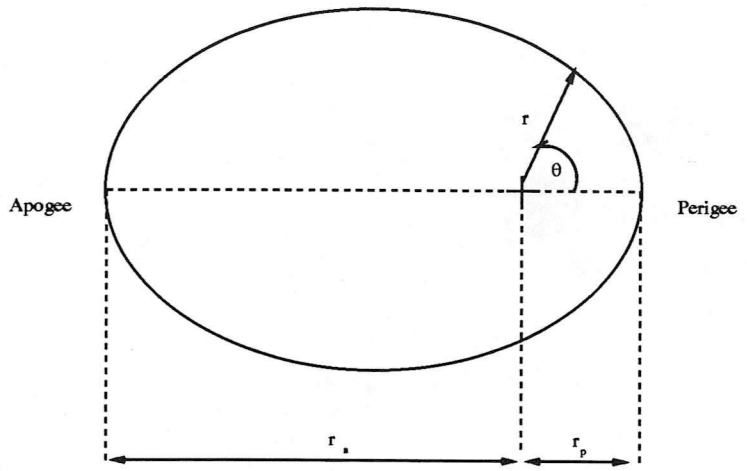

Figure 3: Definition of a and e on elliptical orbit.

- Inclination, i the angle between the plane of the orbit and the equatorial plane

- Argument of Perigee, ω the angle between the equator crossing point and the perigee. (the point of closest approach to the earth)

- Right Angle of the Ascending Node Ω, the angle between the x-axis and the line joining the equator crossing points (the so-called "line of nodes").

- True Anomaly, θ is the angle between the satellite's position at time, t and its perigee position.

A further parameter, the time of perigee passage, τ is required to fix the satellite's position in time.

The effect of perturbing forces such as air drag and gravitational harmonics on the orbital elements may be calculated directly using Lagrange's Planetary Equations. This method offers considerable speed advantages over the integration of cartesian coordinates, and eliminates the need for orbital elements to be calculated directly from the position and velocity vectors.

The classical element set desribed above, $[a\ e\ i\ \omega\ \Omega]$ becomes singular when either e or i are zero, due to the indeterminacy of ω and Ω. When modelling satellite constellations, near-circular orbits are of obvious interest and the eccentricity singularity becomes a problem. To eliminate the singularities, an element set which removes the singularities is required. The

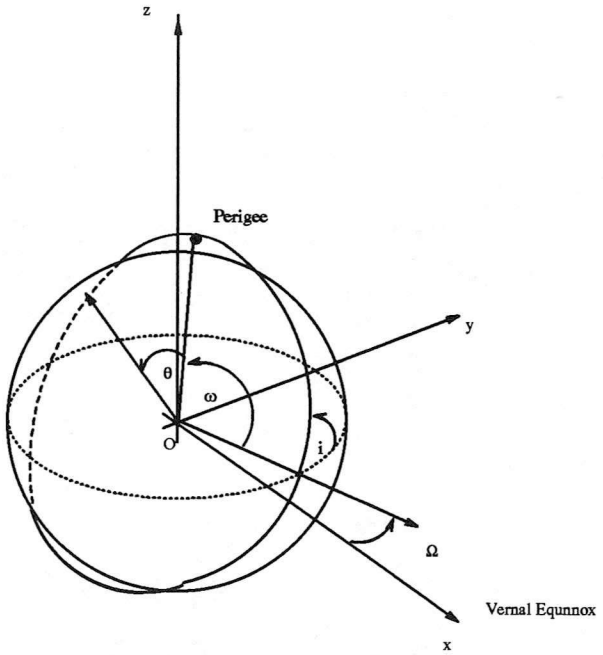

Figure 4: Orbital Geometry in GCI system

equinoctial set, described by Battin,[10] is a suitable choice,

$$a \tag{3a}$$
$$P_1 = e\cos\varpi \tag{3b}$$
$$P_2 = e\sin\varpi \tag{3c}$$
$$Q_1 = \tan i/2 \sin\Omega \tag{3d}$$
$$Q_2 = \tan i/2 \cos\Omega \tag{3e}$$

where ϖ is the argument of perigee, measured from the node given by:

$$\varpi = \omega + \Omega \tag{4}$$

The mean anomaly,

$$l = n(t-\tau) + \varpi \tag{5}$$

completes the set.

2.2 Model Derivation

2.2.1 Lagrange Planetary Equations

Lagrange's Planetary Equations describing the effects of accelerations on the elements of equation 3a are given by the following equations (derived in

Appendices A and B).

$$\frac{da}{dt} = \frac{2a^2}{h}\left[(P_2 \sin L - P_1 \cos L)a_{dr} + \frac{p}{r}a_{d\theta}\right] \tag{6a}$$

$$\frac{dP_1}{dt} = \frac{r}{h}\Big[-\frac{p}{r}\cos L a_{dr} + \left[P_1 + \left(1+\frac{p}{r}\right)\sin L\right]a_{d\theta} - P_2(Q_1 \cos L - Q_2 \sin L)a_{dn}\Big] \tag{6b}$$

$$\frac{dP_2}{dt} = \frac{r}{h}\Big[-\frac{p}{r}\sin L a_{dr} + \left[P_2 + \left(1+\frac{p}{r}\right)\right]a_{d\theta} - P_1(Q_1 \cos L - Q_2 \sin L)a_{dn}\Big] \tag{6c}$$

$$\frac{dQ_1}{dt} = \frac{r}{2h}(1+Q_1^2+Q_2^2)\sin L a_{dn} \tag{6d}$$

$$\frac{dQ_2}{dt} = \frac{r}{2h}(1+Q_1^2+Q_2^2)\cos L a_{dn} \tag{6e}$$

$$\frac{dl}{dt} = n - \frac{r}{h}\Big[\left(\frac{a}{a+b}\frac{p}{r}(P_1 \sin L + P_2 \cos L) + \frac{2b}{a}\right)a_{dr} + \frac{a}{a+b}\left(1-\frac{p}{r}\right)(P_1 \cos L - P_2 \sin L)a_{d\theta} + (Q_1 \cos L - Q_2 \sin L)a_{dn}\Big] \tag{6f}$$

where

$$b = a\sqrt{1-P_1^2-P_2^2} \tag{7}$$

$$h = nab \tag{8}$$

$$\frac{p}{r} = 1 + P_1 \sin L + P_2 \cos L \tag{9}$$

$$\frac{r}{h} = \frac{h}{\mu(1+P_1 \sin L + P_2 \cos L)} \tag{10}$$

$$\sin L = \frac{a}{r}\left[\left(1-\frac{a}{a+b}P_2^2\right)\sin K + \frac{a}{a+b}P_1 P_2 \cos K - P_1\right] \tag{11}$$

$$\cos L = \frac{a}{r}\left[\left(1-\frac{a}{a+b}P_2^2\right)\cos K + \frac{a}{a+b}P_1 P_2 \sin K - P_2\right] \tag{12}$$

$$K = l - P_1 \sin K + P_2 \cos K \tag{13}$$

a_{dr}, $a_{d\theta}$ and a_{dn} are the disturbing accelerations in the radial, tangential and normal directions, respectively (see Figure 5).

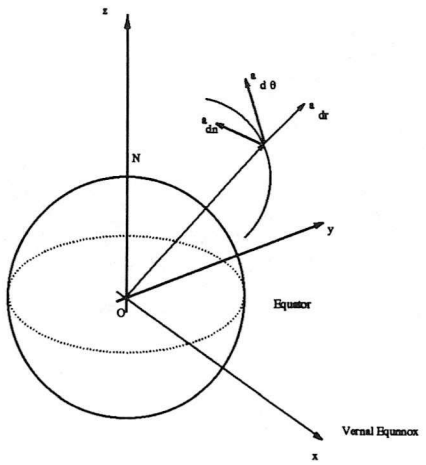

Figure 5: Geometry of accelerations in Equation 6a

2.2.2 Drag Model

Air Drag is modelled acting solely along the tangential direction. The acceleration due to air drag is given by

$$a_{d\theta} = -\frac{\rho V^2}{2\beta} \tag{14a}$$

$$= a_{drag} \tag{14b}$$

$$a_{dr} = 0 \tag{14c}$$

$$a_{dn} = 0 \tag{14d}$$

The Ballistic coefficient, β is defined as

$$\beta = \frac{SC_D}{m} \tag{15}$$

where S is satellite cross-sectional area, C_D is drag coefficient and m is mass. The atmospheric density is modelled on an exponential profile based on data given in King-Hele.[11]

$$\rho = \rho_0 \exp\left[\frac{r - R_e}{H}\right] \tag{16}$$

where ρ_0 is base density ($1.225 kg/m^3$), H is the scale height ($13.5 km$ for $400 km$ altitude) and R_e is the Earth's radius ($6371 km$). Finally, the velocity, V is given by the familiar expression for velocity on a elliptical Keplerian orbit.

$$V = \sqrt{\frac{2\mu}{r} - \frac{\mu}{a}} \tag{17}$$

Substituting Equations 14a into 6a gives

$$\frac{da}{dt} = \frac{2a^2}{h}\frac{p}{r}a_{drag} \tag{18a}$$

$$\frac{dP_1}{dt} = \frac{r}{h}\left[\left(P_1 + \left(1+\frac{p}{r}\right)\sin L\right)a_{drag}\right] \tag{18b}$$

$$\frac{dP_2}{dt} = \frac{r}{h}\left[\left(P_2 + \left(1+\frac{p}{r}\right)\cos L\right)a_{drag}\right] \tag{18c}$$

$$\frac{dQ_1}{dt} = 0 \tag{18d}$$

$$\frac{dQ_2}{dt} = 0 \tag{18e}$$

$$\frac{dl}{dt} = n - \frac{r}{h}\left[\frac{a}{a+b}\left(1-\frac{p}{r}\right)(P_1\cos L - P_2\sin L)\right]a_{drag} \tag{18f}$$

2.2.3 J_2 Effects

The mean effects of the J_2 harmonic are confined to the elements ω and Ω, viz

$$\dot{\varpi} = \frac{3}{4}J_2\left(\frac{p}{R_e}\right)^2 n(5\cos^2 i - 1) \tag{19a}$$

$$\dot{\Omega} = -\frac{3}{2}J_2\left(\frac{p}{R_e}\right)^2 n\cos i \tag{19b}$$

The mean effects of J_2 on the equinoctial elements may be calculated through the chain rule e.g for P_1

$$\frac{dP_1}{dt} = \frac{\partial P_1}{\partial \varpi}\dot{\varpi} + \frac{\partial P_1}{\partial e}\dot{e} \tag{20}$$

The rates of change of the complete Equinoctial set are calculated as:

$$\frac{da}{dt} = 0 \tag{21a}$$

$$\frac{dP_1}{dt} = P_2 J_2\left(\frac{R_e}{p}\right)^2\left(-\frac{3}{2}\cos i + \frac{3}{4}(5\cos^2 i - 1)\right) \tag{21b}$$

$$\frac{dP_2}{dt} = -P_1 J_2\left(\frac{R_e}{p}\right)^2\left(-\frac{3}{2}\cos i + \frac{3}{4}(5\cos^2 i - 1)\right) \tag{21c}$$

$$\frac{dQ_1}{dt} = -\frac{3}{2}Q_2 J_2\left(\frac{R_e}{p}\right)^2 ncosi \tag{21d}$$

$$\frac{dQ_2}{dt} = \frac{3}{2}Q_1 J_2\left(\frac{R_e}{p}\right)^2 ncosi \tag{21e}$$

$$\frac{dl}{dt} = \frac{3}{4}J_2\left(\frac{R_e}{p}\right)^2 n(5\cos^2 i - 1) \tag{21f}$$

Combining the results of the equations 18 and 21 gives the complete coupled equations for the effects of J_2 and drag on the Equinoctial elements.

$$\frac{da}{dt} = \frac{2a^2}{h}\frac{p}{r}a_{drag} \tag{22a}$$

$$\frac{dP_1}{dt} = \frac{r}{h}\left[\left(P_1 + \left(1+\frac{p}{r}\right)\sin L\right)a_{drag}\right] + P_2 J_2 \left(\frac{R_e}{p}\right)^2 \left(-\frac{3}{2}\cos i + \frac{3}{4}(5\cos^2 i - 1)\right) \tag{22b}$$

$$\frac{dP_2}{dt} = \frac{r}{h}\left[\left(P_2 + \left(1+\frac{p}{r}\right)\cos L\right)a_{drag}\right] - P_1 J_2 \left(\frac{R_e}{p}\right)^2 \left(-\frac{3}{2}\cos i + \frac{3}{4}(5\cos^2 i - 1)\right) \tag{22c}$$

$$\frac{dQ_1}{dt} = -\frac{3}{2}Q_2 J_2 \left(\frac{R_e}{p}\right)^2 ncosi \tag{22d}$$

$$\frac{dQ_2}{dt} = \frac{3}{2}Q_1 J_2 \left(\frac{R_e}{p}\right)^2 ncosi \tag{22e}$$

$$\frac{dl}{dt} = n - \frac{r}{h}\left[\frac{a}{a+b}\left(1-\frac{p}{r}\right)(P_1\cos L - P_2\sin L)a_{drag} + \frac{3}{4}J_2\left(\frac{R_e}{p}\right)^2 n(5\cos^2 i - 1)\right]$$

The model derived above is valid for low, circular Earth orbits as the simple exponential atmospheric drag model is valid only around the chosen reference height and the limited gravity model ignores effects such as J_3, important for the long-term evolution of eccentricity, as well as sectoral and tesseral harmonics which are significant for the evolution of long period orbits. Other effects ignored by this model include, differential drag between different rings caused by the presence of the noon atmospheric density bulge and the inertial orientation of constellation member's solar arrays and the effects of lunisolar gravational perturbations and solar radiation pressure forces, effects which become significant at high altitudes. Future work considering high altitude, or highly elliptic orbits, will require the development of a detailed earth satellite model incorporating these effects.

3 Application of Potential Methods to Orbit Control

3.1 Fundamentals of Potential Control

The Potential function method has been previously been applied to a number of spacecraft control problems.[12] Particular interest has been shown in the application of the method to multi-body proximity operations, such as path-constrained rendezvous and space-assembly operations,[13,14] other applications of the technique have included controlling constrained attitude slews[15] and control of planar rings of satellites.[9]

The method, which originated in terrestrial robotics, is based on defining a scalar potential, Φ. This function is defined to have a global minima corresponding to some required terminal state, within regions to be avoided the potential is defined to have some large value. In previous applications, controls have been selected, to satisfy the Lyupanov stability criterion

$$\frac{d\Phi}{dt} < 0 \tag{23}$$

ie the rate of change of the potential is negative definite (the system is therefore converging to the desired terminal state). For orbit control applications the very low sampling rates (on the order of hours) and step changes in state variables (ie the orbital element vector $\boldsymbol{\alpha} = [a\ e\ i\ \omega\ \Omega]^T$) make a different form appropriate.

Write equation 23 in a time-differenced form,

$$\Phi(t) - \Phi(t - \Delta t) < 0 \tag{24}$$

where Δt is the time period between separate samples of the potential. The conditon for stability is now that the potential must fall over the time interval between sample points. This equation may be used as the switching criterion for an impulsive control.

$$s(t) = \begin{cases} 0 & \text{if } \Phi(t) - \Phi(t - \Delta t) > 0 \\ 1 & \text{if } \Phi(t) - \Phi(t - \Delta t) \leq 0 \end{cases} \tag{25}$$

When $s(t) = 1$, a step change in the element vector, α is made along the direction of steepest descent:

$$\Delta\boldsymbol{\alpha} = -\boldsymbol{\kappa}\frac{\nabla\Phi}{\|\nabla\Phi\|} \tag{26}$$

This control permits the system dynamics to freely propagate until the potential rises, at which point the control pushes the system in the direction that will cause the potential to be lowered, forcing the system towards convergence with the global minimum.

The convergence of the control law of 25 will now be shown by considering a first order Taylor series expansion of 24, ignoring time dependent terms:

$$\Phi(t) - \Phi(t - \Delta t) \approx \frac{\partial \Phi}{\partial \alpha_1}\Delta\alpha_1 + \ldots + \frac{\partial \Phi}{\partial \alpha_n}\Delta\alpha_n \quad (27)$$

$$= \nabla\Phi.\Delta\boldsymbol{\alpha} \quad (28)$$

Substituting 26 into the above, an expression for the change in potential caused by the control input is

$$\Delta V = -\nabla\Phi.\boldsymbol{\kappa}\frac{\nabla\Phi}{\|\nabla\Phi\|} \quad (29)$$

In previous applications $\boldsymbol{\kappa}$ has been scalar constant and it is easy to see that the above equation reduces to,

$$\Delta\Phi = -\kappa\|\nabla\Phi\| \quad (30)$$

so that convergence is assured if κ is positive definite. However, for orbit control applications, control variables such as a and e have different orders of magnitude, under these circumstances κ should be considered to be a matrix term,

$$\boldsymbol{\kappa} = \begin{bmatrix} \kappa_{11} & \ldots & \kappa_{1n} \\ \vdots & \ddots & \vdots \\ \kappa_{n1} & \ldots & \kappa_{nn} \end{bmatrix} \quad (31)$$

If we consider Equation 29 again, with the matrix form of κ given above, then

$$\Delta\Phi = \frac{1}{\|\Phi\|}\left[\kappa_{11}\left(\frac{\partial\Phi}{\partial\alpha_1}\right)^2 + \ldots + \kappa_{1n}\frac{\partial\Phi}{\partial\alpha_n}\frac{\partial\Phi}{\partial\alpha_1} + \right.$$

$$\left. \ldots + \kappa_{n1}\frac{\partial\Phi}{\partial\alpha_n}\frac{\partial\Phi}{\partial\alpha_1} + \cdots + \kappa_{nn}\left(\frac{\partial\Phi}{\partial\alpha_n}\right)^2\right] \quad (32)$$

For convergence, it is required to have $\Delta\Phi$ positive definite, this condition may be met if the leading diagonal terms of κ are positive definite and the non-diagonal terms are zero. The case where κ was a scalar constant can clearly be seen to be equivalent to $\boldsymbol{\kappa} = \kappa\boldsymbol{I}$.

3.2 Implementation

This section discusses the implementation of the control method in an closed, onboard control loop, with regard to issues such as navigational measurements and inter-satellite links.

To provide fully autonomous orbit control, the guidance system must be provided with navigational data independent of ground tracking. Recent developments in satellite borne GPS systems[16,17] allow the spacecraft to gather positional data, in and estimate its orbital elements, in real time. A further advantage of GPS is that navigational data is available continously, and not just when the satellite is visible from a ground station.

It is assumed that the orbital elements output by the GPS system may be filtered to provide mean rather than the (instantaneous) osculating elements, which vary over an orbital period. For spacecraft with limited onboard resources, savings in power and processor time may be achieved operating the GPS reciever intermittently, with an analytic orbit propagator being used to estimate elements during the time period between GPS updates.[17]

A number of advanced constellation designs feature inter-satellite links (ISLs). These links are designed to allow the satellites to pass user communications signals to one another, but in in theory should be allow the satellites to exchange positional data with the rest of the constellation. Most of the constellations lack such links and feature "bent pipe" links through ground stations, however, it may be possible to transmit data across the constellation through these links.

The inter-satellite links pose a number of interesting questions regarding the design of a constellaton-wide distributed control system. For very large constellations the memory required to store the relative positions of all the satellites could prove prohibitive. Furthermore, consideration must be given to the update frequency to avoid using a significant amount of communications bandwidth for the constellation's navigational purposes. Ways of alleviating these problems, such as designing control laws that control the phasing of adjacent satellites only, will be considered by future studies.

A schematic of the control system is shown in Figure 6. The GPS system feeds mean elements, to the Potential Function Control which uses this data together with the reference orbit elements and inter-satellite phasing data to evaluate possible control inputs, as described earlier. The output of the control, in the form of a required change in orbital elements, is input into the $\Delta\Phi$ logic. The element changes are converted into a change in velocity through Equations 33

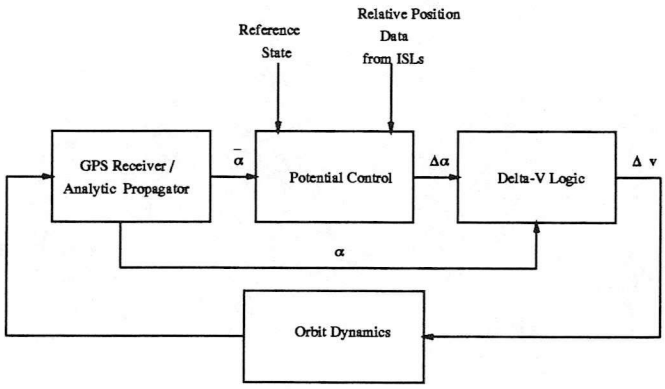

Figure 6: Schematic of Potential Control Scheme

$$\Delta a = \frac{2a^2}{h}\left[(P_2 \sin L - P_1 \cos L)\Delta v_r + \frac{p}{r}\Delta v_\theta\right] \tag{33a}$$

$$\Delta P_1 = \frac{r}{h}\Big[-\frac{p}{r}\cos L \Delta v_r + \left(P_1 + \left(1+\frac{p}{r}\right)\sin L\right)\Delta v_\theta - P_2(Q_1 \cos L - Q_2 \sin L)\Delta v_n\Big] \tag{33b}$$

$$\Delta P_2 = \frac{r}{h}\Big[-\frac{p}{r}\sin L \Delta v_r + \left[P_2 + \left(1+\frac{p}{r}\right)\cos L\right]\Delta v_\theta - P_1(Q_1 \cos L - Q_2 \sin L)\Delta v_n\Big] \tag{33c}$$

$$\Delta Q_1 = \frac{r}{2h}(1 + Q_1^2 + Q_2^2)\sin L \Delta v_n \tag{33d}$$

$$\Delta Q_2 = \frac{r}{2h}(1 + Q_1^2 + Q_2^2)\cos L \Delta v_n \tag{33e}$$

$$\Delta l = n - \frac{r}{h}\Bigg[\left(\frac{a}{a+b}\frac{p}{r}(P_1 \sin L + P_2 \cos L) + \frac{2b}{a}\right)\Delta v_r + \frac{a}{a+b}\left(1-\frac{p}{r}\right)(P_1 \cos L - P_2 \sin L)\Delta v_\theta + (Q_1 \cos L - Q_2 \sin L)\Delta v_n\Bigg] \tag{33f}$$

Obviously, with 6 equations and 3 control variables only a sub-set of the variables may be controlled. For the purposes of this study it will be assumed that thrusters are available in the radial and tangential directions, direct control of a and e will therefore only be possible. It will be shown later how the elements ω and Ω may be indirectly controlled via the effects of J_2.

The effect of the step change in e on the variable P_1 is obtained by a

Taylor series expansion

$$\begin{aligned}\Delta P_1 &= \frac{\partial P_1}{\partial e}\Delta e \\ &= \sin\varpi\Delta e\end{aligned} \tag{34}$$

The first 2 equations of 33 written in matrix form, neglecting Δv_n terms are

$$\begin{bmatrix}\Delta a \\ \Delta P_1\end{bmatrix} = \begin{bmatrix}\frac{2a^2}{h}(P_2\sin L - P_1\cos L) & \frac{2a^2}{h}\frac{p}{r} \\ -\frac{r}{h}\frac{p}{r}\cos L & \frac{r}{h}\left(P_1 + \left(1+\frac{p}{r}\right)\sin L\right)\end{bmatrix}\begin{bmatrix}\Delta v_r \\ \Delta v_\theta\end{bmatrix}$$
$$\Delta\alpha = C\Delta\mathbf{v} \tag{35}$$

This matrix term in this equation may be inverted to give the required velocity change vector.

$$\Delta v = C^{-1}\Delta\alpha \tag{36}$$

In the future, the controls could be extended to include burns normal to the orbital plane to provide control over inclination. Care must however be taken to ensure that the controls are triggered at points on the orbit where the C matrix is non-singular.

Although ignored for the purposes of this work, the ΔV logic must also convert the Δv vector from the local LVLH frame of reference into the body axes and select thrusters and firing time accordingly.

4 Control of Single Satellites

4.1 Orbit Maintenance

This section describes the maintainance of the orbit of a single satellite against the perturbing effects of air drag using the control scheme previously described. The Potential is based on the difference between semi-major axis and the reference semi-major axis.

$$\Phi = \lambda_a (a - \overline{a})^2 \tag{37}$$

where λ_a is a constant scaling parameter. In practice, due to noise in navigational measurements and thruster accuracy, it will only be possible to control a within some limit, or deadband. This may be accomplished by placing a flat "floor" into the potential about the reference point as shown in Figure 7, where the width of the deadband region is $2a_{db}$. Within the deadband if

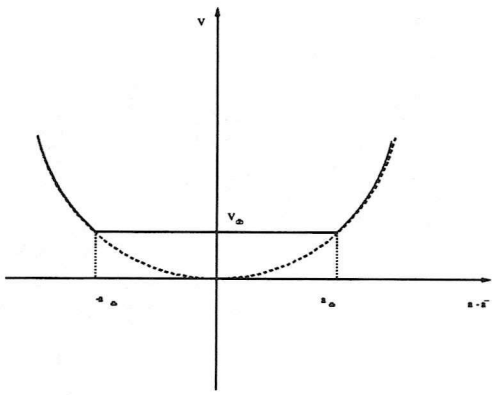

Figure 7: Potential Function with deadband around reference point

the control activates it is obvious that $\frac{\partial V}{\partial a} = 0$ and no change in a will be commanded by the control ie the spacecraft will be allowed to drift freely within this region.

Mathematically, the potential may be written as:

$$\Phi = \frac{\lambda_a}{2} \begin{cases} (a - \overline{a})^2 & (a - \overline{a}) \geq a_{db} \\ a_{db}^2 & (a - \overline{a}) < a_{db} \end{cases} \tag{38}$$

The partial derivative of this expression with respect to a is then

$$\frac{\partial \Phi}{\partial a} = \lambda_a \begin{cases} (a - \overline{a}) & (a - \overline{a}) \geq a_{db} \\ 0 & (a - \overline{a}) < a_{db} \end{cases} \tag{39}$$

where λ_a is a scaling parameter.

The control derived above will now be applied to the drag maintenance of a satellite ($\beta = 0.011m^2kg^{-1}$) in a circular, $400km$ orbit. The control has a semi-major axis deadband width of $80m$, with $\lambda_a = 1$, $\kappa_a = 120$ and is sampled every $1000s$.

The semi-major axis histories for controlled and uncontrolled cases are shown in Figure 8. The control allows the semi-major axis to decay until the spacecraft reaches the lower limits of the deadband where an impulse is applied to increase the semi-major axis.

The eccentricity results of Figure 9 show only small errors in e due to the approximation of Equation 34, these errors in eccentricity are extremely small (of the order of $10E-4$) and are of little significance. However, for applications which require a frozen orbit, the variation in argument of perigee indicated in 9 is of some concern as the control has a substantial effect on this parameter. This result is unsurprising, since there are three in-plane elements (a, e and ω) and only two in-plane controls acting on them. With this scheme it will therefore only possible to directly control two elements, this problem may be alleviated by a multiple burn scheme (e.g. at perigee and apogee).

The cumulative Δv results are compared with the optimal value calculated from the acceleration required to eliminate the effects of drag, in Figure 10. It can be seen that the control applies an impulse of around $8cms^{-1}$ approximately every 4.5 days. The near-optimality of the control can clearly be seen, suggesting that the ΔV cost is largely unaffected by the off-optimal burn times.

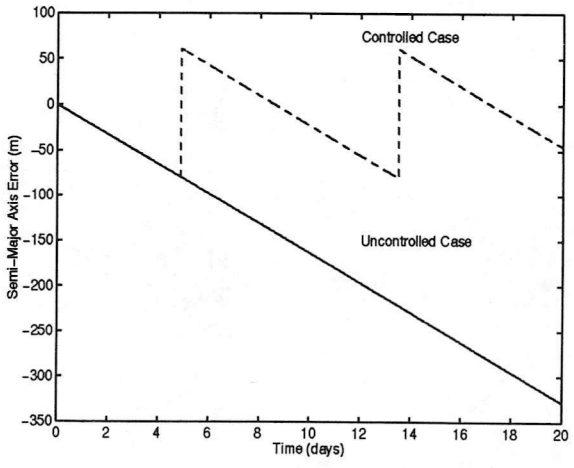

Figure 8: Semi-Major axis time histories. Controlled and Uncontrolled cases

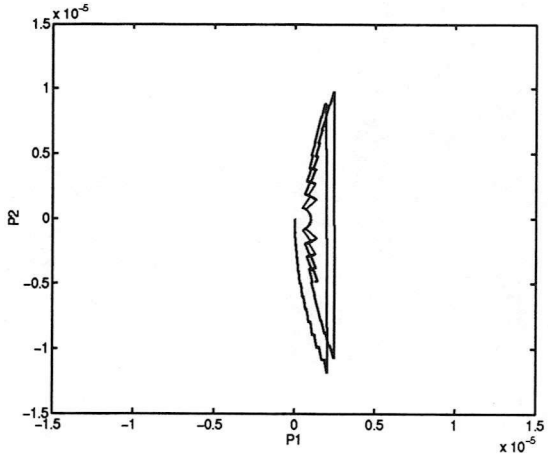

Figure 9: Evolution of Eccentricity vector, controlled case.

4.2 Orbit Manouevring

In this section, a rudimentary orbit manouevring capability will be demonstrated. The reference value of semi-major axis is ramped from $6671km$ to $6671.5km$ over a period of 10 days. The control parameters are as specified in the previous section.

Figure 11 shows the semi-major axis history, as the reference semi-major axis ramps up an increased frequency of impulsive burns is evident (approximately every 1.8 days) due to the base of the deadband rising to meet the spacecraft. After 10 days the deadband base ceases to rise and the control begins the station keeping cycle seen earlier. These results can also be clearly seen in the ΔV history of Figure 12.

Figure 13 shows the evolution of the eccentricity vector. As in the previous case, both eccentricity and argument of perigee are seen to be affected by the control. Errors in e can be seen to rise to larger levels than in the previous case, due to the increased burn frequency.

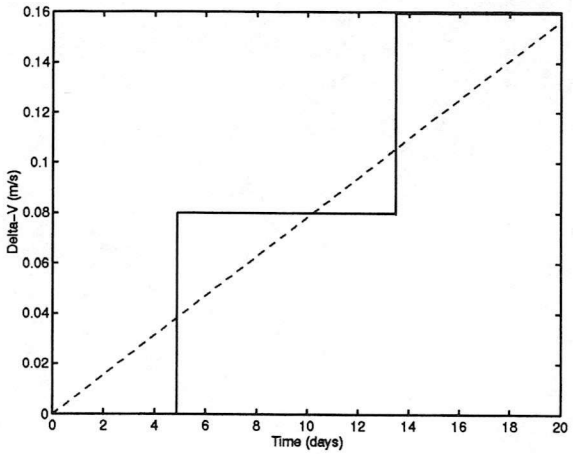

Figure 10: Comparison of Δv costs of a-control and optimal drag make up.

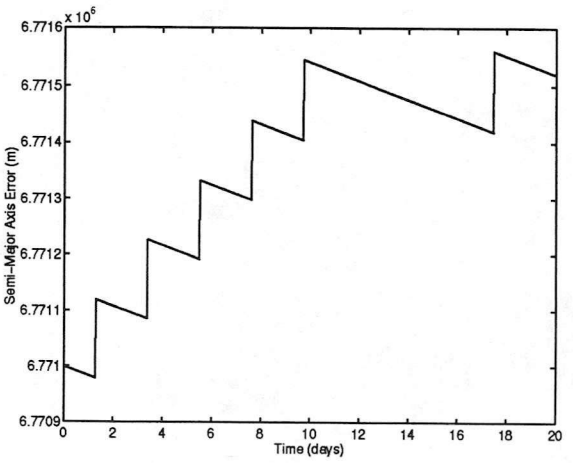

Figure 11: Semi-major axis history, orbit raising case.

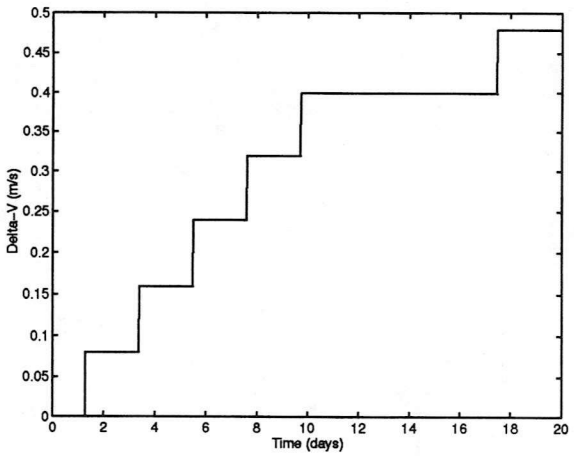

Figure 12: ΔV history, orbit raising case.

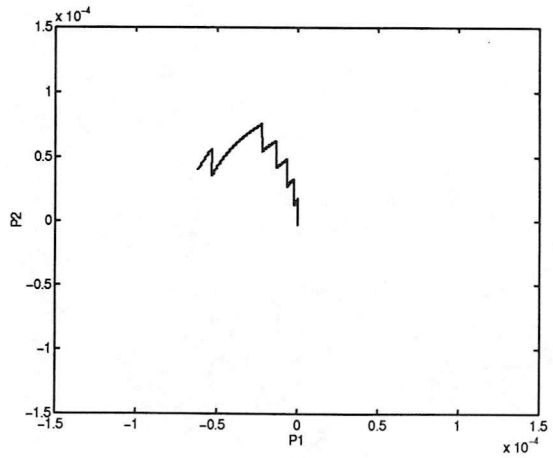

Figure 13: Evolution of Eccentricity vector, orbit raising case.

5 Constellation Phasing Control

5.1 Indirect Phasing Control

In order to derive a phasing control it is necessary to specify a measure of the inter-satellite phasing angle. At first sight basing this measure on true anomaly would seem a logical choice, however this angle is not explicitely linked to the orbital elements which makes the calculation of derivatives impossible. The Mean Anomaly (Equation 40)

$$M = n(t - \tau) \tag{40}$$

is a better choice of angular measure as it may be explicitly linked to a. For near-circular orbits the error between Mean and True Anomaly is very small as can be clearly seen in Figure

The phase angle is defined as

$$\phi = M + \omega - \bar{n}t \tag{41}$$

where $\bar{n}$ is the reference orbital rate of the constellation. At this point it is also useful to define the mean inter-satellite spacing,

$$\bar{\phi} = \frac{1}{N-1} \sum_{i=1}^{N} \phi_i \tag{42}$$

for a ring of N satellites. As the rate of change of the phase angle is governed by a, it can be observed that if satellites have differing rates of decay then an initially evenly spaced ring will degrade with time. Such differential drag effects can be caused either by differing Ballistic Coefficients or local variations in atmospheric density.

The results of the effects of differential drag caused by a variation of β of $\pm 10\%$ are shown in Figure 14 for a 3-satellite ring at $400km$ altitude. The drag causes the constellation spacing to degrade over time. Adding the semi-major axis control derived in the previous section can be seen to prevent this loss of even spacing.

Clearly a small variation in Ballistic coefficient can to cause substantial changes in mean phasing for low (400km) orbits, it can be seen that controlling the semi-major axis to some deadband limit can maintain a constellation's relative phasing.

5.2 Direct Phasing Control

The previous section showed that an initially evenly spaced constellation could be maintained against perturbing forces using the controls derived in

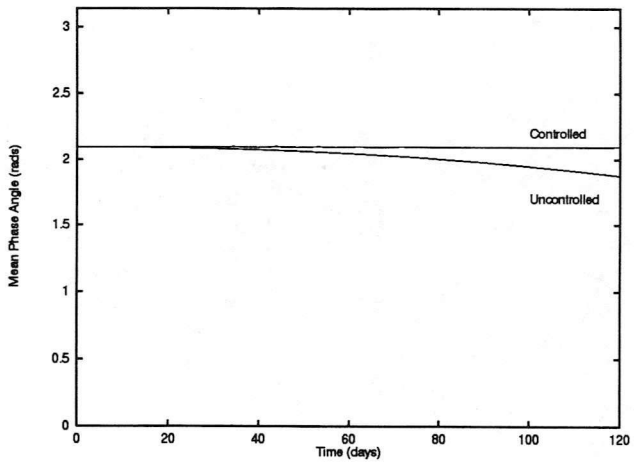

Figure 14: Evolution of Mean Spacing for a 3-satellite ring. Controlled and Uncontrolled cases.

the previous section to indirectly maintain spacing. In this section a direct method for controlling the spacing of a ring of satellites will be derived. As discussed in the Introduction, such a control method should be able to reform the constellation in the event of the loss of a satellite, or reform the constellation after the introduction of a new member or an on-orbit spare.

A potential of the form

$$\Phi = f(a,e) + g(\phi) \tag{43}$$

will be used. The first term will be that derived in the previous chapter, viz

$$\begin{aligned} f(a,e) = &\frac{\lambda_a}{2}\begin{cases}(a-\overline{a})^2 & (a-\overline{a}) \geq a_{db} \\ a_{db}^2 & (a-\overline{a}) < a_{db}\end{cases} \\ &+ \frac{\lambda_e}{2}\begin{cases}(e-\overline{e})^2 & (e-\overline{e}) \geq e_{db} \\ e_{db}^2 & (e-\overline{e}) < e_{db}\end{cases} \end{aligned} \tag{44}$$

which will act to force the system towards the desired reference elements. The second term in the potential acts to force the satellites to assume an evenly spaced ring. This term is defined, by noting that the potential should assume a high value around each satellite in the ring and is required to be periodic, such that $g(\phi) = g(\phi + 2\pi)$ A suitable potential, with deadband, is for the ith satellite:

$$g_i(\phi_i) = \kappa_\phi \sum_{\substack{j=1 \\ j\neq j}}^{N} \begin{cases}\csc^2 \frac{\phi_{ij}}{2} & \overline{\phi} - \overline{\phi}_{ref} \geq \overline{\phi}_{db} \\ 0 & \overline{\phi} - \overline{\phi}_{ref} < \overline{\phi}_{db}\end{cases} \tag{45}$$

where the phase angle between satellites i and j is given by

$$\phi_{ij} = \phi_i - \phi_j \tag{46}$$

and the mean spacing of an N-satellite ring is given by

$$\overline{\phi}_{ref} = \frac{2\pi}{N} \tag{47}$$

The partial derivatives of the potential will now be evaluated. When evaluating $\nabla\Phi$, the aim is to estimate the gradient over time time interval between samples of the control. Note that

$$\frac{\partial g_i}{\partial a} = \frac{\partial \phi}{\partial a}\frac{\partial g_i}{\partial \phi} \tag{48}$$

Over the time interval, Δt, ϕ changes according to

$$\phi = \phi(t) + \dot{\phi}\Delta t \tag{49}$$

differentiating (49) and substituting into (48) gives

$$\frac{\partial g_i}{\partial a} = \frac{\partial \dot{\phi}_i}{\partial a}\frac{\partial g}{\partial \phi}\Delta t \tag{50}$$

Using Equation 50 to evaluate the a-partial derivative of gives

$$\frac{\partial g}{\partial a} = \Delta t \frac{\partial \dot{\phi}_{ij}}{\partial a} \kappa_\phi \sum_{\substack{j=1 \\ j\neq j}}^{N} \begin{cases} \csc^2\frac{\phi_{ij}}{2}\tan\frac{\phi_{ij}}{2} & \overline{\phi} - \overline{\phi}_{ref} \geq \overline{\phi}_{db} \\ 0 & \overline{\phi} - \overline{\phi}_{ref} < \overline{\phi}_{db} \end{cases} \tag{51}$$

with similar expressions for the e derivative. Note that the $\frac{\partial \dot{\phi}}{\partial a}$ acts to link the natural orbital dynamics (the central body attraction and J_2) with the control. It should be possible to use this feature of the method to add control of Ω via control of inclination to allow full control of a spacecraft orbit in 3D. Applications of this could include maintenance of a sun-synchronous condition, or, for constellation control applications, maintain the separation of adjacent planes.

Figures 15 to 18 show the results of the control applied to a 3-satellite ring. Figure 15 shows the semi-major axis histories of the three spacecraft. Up to 5 days after the start the mean phasing shown in 16 is such that the phasing control is active and the semi-major axes are raised or lowered depending on the required change in phase angle. At this point, the phasing term disappears from the potential and the system begins the station-keeping cycle seen previously. Examination of the semi-major axis history shows that

at around 1.5 days, the phasing potential has fallen to a point where the semi-major axis error term begins to dominate, at this point the semi-major axis errors have reached their maximum values of of $\mp 2500m$. From this point on, the semi-major axis error term acts to push the satellites towards their reference values, consequently a drop in the rate of change of mean phasing is evident from around 2 days.

The ΔV results of Figure 17 show a significant distribution in fuel cost between the satellites. The satellites with the lowest cost are the spacecraft the shows little, or no, change in its phase angle (see Figure 18 being roughly equidistant from the other two satellites. and the satellite which used air drag to lower its semi-major axis during the last 2 days of the rephasing (Figure 15). However, the ΔV costs are low ($< 1.5ms^{-1}$) and could be improved by the modifications to the potential discussed below.

Comparing these results with those of the distributed control derived by McInnes[9] show that this control scheme converges at a higher rate and can cope with greater initial errors.

These results show a number of shortcomings in the method as it currently stands. Firstly, building the potential from a sum of terms due to each satellite leads to the satellites to interact in such a way that the control fires on a continual basis. Although the sum of the bodies' potentials decreases steadily, individual bodies may experience rises in potential, this leads to the continuous changes in semi-major axis evident in Figure 15. Although the system converges, this kind of behaviour is wasteful of fuel and should probably be avoided. Furthermore, the non-linear nature of the potential makes it difficult to reliably select scaling parameters, particularly if satellite numbers change.

A possible solution to these problems is to adopt a "Figure of Merit" approach, in this case the potential would be based on some parameter which decreases steadily as the system converges e.g. the minimum separation between a satellite and its neighbours. This may also alleviate some of the information processing difficulties discussed in a previous section by reducing the number of satellites which have to be tracked by an individual spacecraft and reduce the computational cost of evaluating the control.

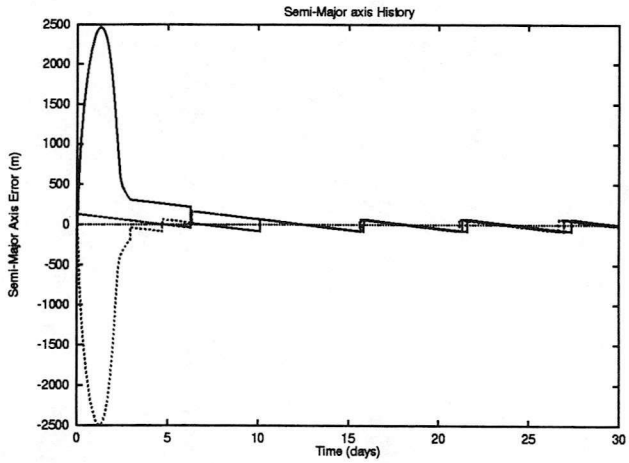

Figure 15: Semi-Major axis histories of rephasing satellites.

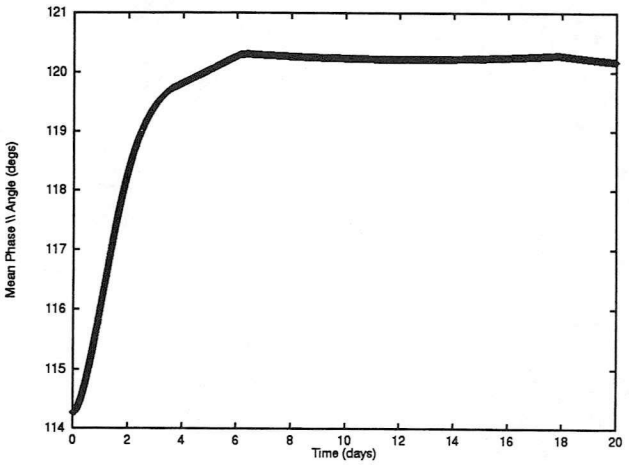

Figure 16: History of Mean Spacing of a 3 satellite ring rephasing under active control.

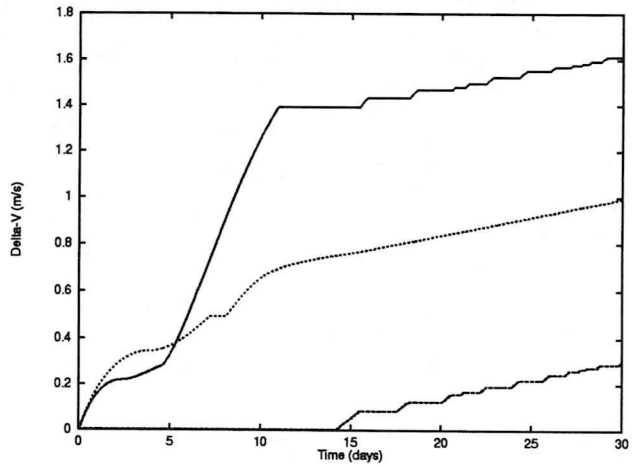

Figure 17: ΔV Histories of 3 satellite ring members during rephasing.

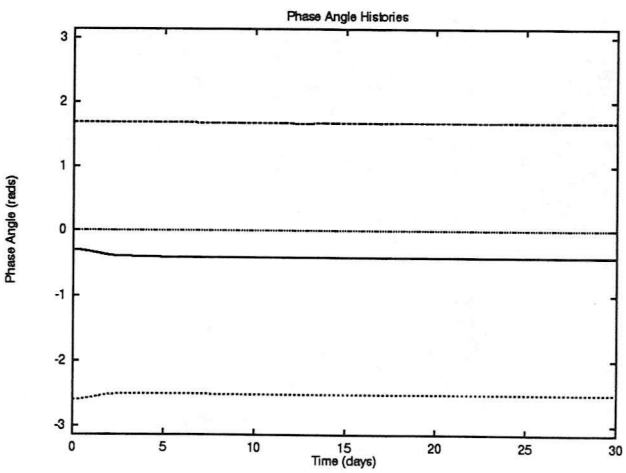

Figure 18: Time History of phase angles for ring members during rephasing.

6 Conclusions and Further Work

The results of this study, demonstrate the feasibility of using Potentials to control a spacecraft's orbit via impulsive changes in velocity. A control strategy has been investigated which is

- Based on Impulsive controls.
- Mathematically validated.
- Not dependent on assumptions of circularity.

Application of the basic methods to both single and multiple satellite cases has been undertaken with some success. The results obtained suggest a number of improvements to the basic method should be undertaken, particularly in the reducing the effects on argument of perigee and reducing the frequency at which the constellation control triggers.

Future work will concentrate on expanding the control to a full 3D form, using J_2 effects to control remaining orbital elements, such as Ω and ω. A control strategy based on Multiple burns (at Perigee, Apogee and equator crossing points could deal with the problems encountered in controlling the orientation of the eccentricity vector allowing fully explicit control of all elements.

Further work on the constellation control to improve the efficiency of the control scheme, replacing the summed potential with a "Figure-of-Merit" based approach, should be undertaken. Demonstrating the applicability of these techniques to elliptic orbits is also a future possibility, however as has been noted elsewhere such work will require a more accurate orbit propagator than has been developed to date.

A Derivation of Lagrange Equations

Lgrange's Planetary equations desribing the variation in the classical elements $[a\ e\ i\ \omega\ \Omega\ M]$ due to the perturbing accelerations (ie those accelerations not due to the inverse-square gravity law) will be derived in this appendix. The derivation which follows is essentially the vector method given by King-Hele.[11]

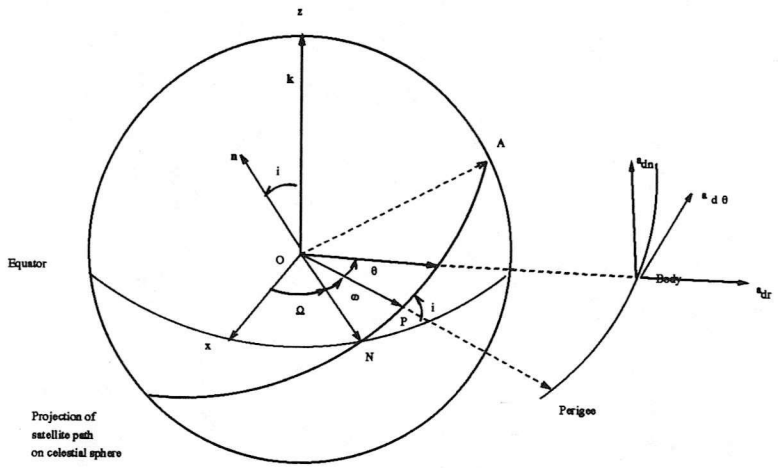

Figure 19: Geometry of Orbital Plane and perturbing accelerations

As the Lagrange equations are derived from considerations of angular momentum and energy, it will be necessary to first derive expressions for the instantaneous values of the position and velocity vectors for a body in orbit around a central body. The differential equation governing a satellite orbit around a primary is

$$\ddot{\mathbf{r}} + \frac{\mu}{r^3}\mathbf{r} = 0 \tag{52}$$

This equation has the solution

$$r = \frac{p}{1 + e\cos\theta} \tag{53}$$

where

$$p = a(1 - e^2) = \frac{h^2}{\mu} \tag{54}$$

The magnitude of angular momentum is given by

$$h = r\dot{\theta}^2 \tag{55}$$

and the angular rate by

$$\dot{\theta} = \frac{\sqrt{\mu p}}{r^2} \tag{56}$$

The transverse velocity component is then calculated as

$$r\dot{\theta} = \frac{\sqrt{\mu p}}{r} = \sqrt{\frac{\mu}{p}}(1 + e\cos\theta) \tag{57}$$

The radial component may easily be found by differentiating equation 53 to give

$$\dot{r} = \frac{p}{1 + e\cos\theta} \tag{58}$$

The radial and velocity vectors are then by equations 53, 57 and 58

$$\mathbf{r} = \left[\begin{array}{ccc} \frac{p}{1+e\cos\theta} & 0 & 0 \end{array} \right]^T \tag{59}$$

$$\mathbf{v} = \left[\begin{array}{ccc} \sqrt{\frac{\mu}{p}} e\sin\theta & \sqrt{\frac{\mu}{p}}(1 + e\cos\theta & 0 \end{array} \right] \tag{60}$$

Having obtained the position and velocity vectors we are now in a position to consider the effects of a perturbing acceleration $\mathbf{a}$ on the orbit. Write equation 52 as

$$\ddot{\mathbf{r}} + \frac{\mu}{r^3}\mathbf{r} = \mathbf{a} \tag{61}$$

The variation in semi-major axis will be calculated first. Differentiating the energy equation

$$\frac{1}{2}\dot{\mathbf{r}}.\dot{\mathbf{r}} = \mu\left(\frac{1}{r} - \frac{1}{2a}\right) \tag{62}$$

gives [1]

$$\frac{1}{\mu}\dot{\mathbf{r}}.\ddot{\mathbf{r}} = -\frac{\mathbf{r}.\dot{\mathbf{r}}}{r^3} + \frac{\dot{a}}{2a^2} \tag{63}$$

[1] since $|\mathbf{r}| = (\mathbf{r}.\mathbf{r})^{\frac{1}{2}}$ the time derivative of $|\mathbf{r}|^{-1}$ is

$$\begin{aligned} \frac{d}{dt}|\mathbf{r}|^{-1} &= \frac{d}{dt}(\mathbf{r}.\mathbf{r})^{\frac{1}{2}} \\ &= -(\mathbf{r}.\dot{\mathbf{r}})(\mathbf{r}.\mathbf{r})^{-\frac{3}{2}} \\ &= -(\mathbf{r}.\dot{\mathbf{r}}r)^{-3} \end{aligned}$$

Rearranging the above equation and substituting 52 gives

$$\frac{da}{dt} = \frac{2a^2}{\sqrt{\mu p}}\mathbf{r}.\mathbf{a} \tag{64}$$

Substituting the acceleration vector

$$\mathbf{a} = \begin{bmatrix} a_{dr} & a_{d\theta} & a_{dn} \end{bmatrix}^T \tag{65}$$

gives the equation for the variation of semi-major axis with time

$$\frac{da}{dt} = \frac{2a^2}{\sqrt{\mu p}}\{a_{dr} e \sin\theta + a_{d\theta}(1 + e\cos\theta)\} \tag{66}$$

The remaining equations are derived from angular momentum arguments. Angular momentum is given by

$$\mathbf{h} = \mathbf{v} \times \mathbf{r} \tag{67}$$

Substituting the previously derived expression for h, and differentiating [2] gives, since $(\mathbf{r} \times \mathbf{r} = 0)$.

$$\dot{\mathbf{n}} + \frac{\dot{p}}{2p}\mathbf{n} = \sqrt{\mu p}\mathbf{r} \times \mathbf{a} \tag{68}$$

Since $\mathbf{n}$ is a unit vector, the rate of change of $\mathbf{n}$ may be written as

$$\dot{\mathbf{n}} = \mathbf{B} \times \mathbf{n} \tag{69}$$

where $\mathbf{B}$ is the angular velocity of $\mathbf{n}$. From Figure 19 it may be seen that the orientation of $\mathbf{n}$ depends on the elements i and Ω, correspondingly $\mathbf{B}$ has components $\dot{\Omega}$ about $\mathbf{k}$ and di/dt about $\overline{ON}$. By inspection of the figure

$$\dot{\mathbf{n}} = \mathbf{B} \times \mathbf{n} = \dot{\Omega}\sin i\overline{ON} - \frac{di}{dt}\overline{OA} \tag{70}$$

$\mathbf{r} \times \mathbf{a}$ is then calculated as

$$\mathbf{r} \times \mathbf{a} = r a_{dn} \sin u\overline{ON} - a_{dn}\cos u\overline{OA} + r a_{d\theta}\mathbf{n} \tag{71}$$

[2] Expanding, and differentiating, the first term of the cross-product on the Right-Hand side of equation 67 gives

$$\begin{aligned} \frac{d}{dt}(r_2\dot{r}_3 - r_3\dot{r}_2) &= r_2\ddot{r}_3 + \dot{r}_2\dot{r}_3 - \dot{r}_2\dot{r}_3 - r_3\ddot{r}_2 \\ &= r_2\ddot{r}_3 - r_3\ddot{r}_2 \end{aligned}$$

Similar expressions may be derived for the other 2 components of the derivative. By inspection it may be seen that this is the first term of the cross product of $\mathbf{r}$ and $\ddot{\mathbf{r}}$.

Substituting the above into 67 and taking components along the normal direction gives the Lagrange equations for i and Ω

$$\frac{d\Omega}{dt} = \sqrt{\mu p}\frac{\sin u}{\sin i}a_{dn} \tag{72}$$

$$\frac{di}{dt} = \sqrt{\mu p}\cos u a_{dn} \tag{73}$$

and the equation for $\dot{p}$.

$$\dot{p} = 2r\sqrt{\frac{p}{\mu}}a_{d\theta} \tag{74}$$

Since $p = a(1-e^2)$

$$\dot{p} = \dot{a}(1-e^2) - 2a\dot{e}e \tag{75}$$

Substituting 74 in 75 and rearranging gives the Lagrange equation for eccentricity.

$$\dot{e} = \left(\frac{p}{\mu}\right)^{\frac{1}{2}}\left(a_{dr}\sin\theta + ((p+r)\cos\theta + re)\,a_{d\theta}\right) \tag{76}$$

To obtain the equation for $\dot{\omega}$, consider the angular momentum of the body about $\mathbf{n}$ due to the angular velocity of the body in the orbital plane, $(\dot{\omega}+\dot{\theta})\mathbf{n}$ and the component of the orbit plane's angular motion along $\mathbf{n}$, $\dot{\Omega}\sin i$. The angular momentum is then

$$\mathbf{h} = r^2(\dot{\omega} + \dot{\theta} + \dot{\Omega}\cos i)\mathbf{n} \tag{77}$$

By comparison with equation 55

$$\dot{\omega} + \dot{\Omega}\cos i = \frac{\sqrt{\mu p}}{r^2} - \dot{\theta} \tag{78}$$

Differentiation of equation 53 with respect to time gives the rate of change of the true anomaly, $\dot{\theta}$ as

$$-\sin\theta\dot{\theta} = -\frac{\dot{e}}{e^2}\left(\frac{p}{r} - 1\right) + \frac{1}{e}\left(\frac{\dot{p}}{r} - \frac{\dot{r}p}{r^2}\right) \tag{79}$$

Substitution of this equation and the previously derived values of $\dot{r}$, $\dot{p}$ and $\dot{e}$ into 78 gives

$$\dot{\omega} + \dot{\Omega}\cos i = \frac{1}{e}\left(\frac{p}{\mu}\right)^{\frac{1}{2}}\left\{\cos\theta a_{dt} + \left(1 + \frac{r}{p}\right)\sin\theta a_{d\theta}\right\} \tag{80}$$

The equation for $\dot{M}$ is derived as follows. The time derivative of the mean anomaly is derived from Kepler's equation as

$$\frac{dM}{dt} = \frac{dE}{dt} - \dot{e}\sin E - e\frac{dE}{dt}\cos E \tag{81}$$

$\dot{e}$ has already been derived. $\sin E$, $\cos E$ and $\frac{dE}{dt}$ can be derived from

$$\cos\theta = \frac{\cos E - e}{1 - e\cos E} \tag{82}$$

$$\sin\theta = \frac{\sqrt{1-e^2}\sin E}{1 - e\cos E} \tag{83}$$

The result is derived as

$$\frac{dM}{dt} = n + \frac{b}{ahe}\left[(p\sin\theta - 2re)a_{dr} - (p+r)\sin\theta a_{d\theta}\right] \tag{84}$$

The full set of equations are summarised below for completeness, (Note that $p = b^2/a$ and $h = nab$).

$$\frac{da}{dt} = \frac{2a^2}{h}\left(e\sin\theta a_{dr} + \frac{p}{r}a_{d\theta}\right) \tag{85a}$$

$$\frac{de}{dt} = \frac{1}{h}\left(p\sin\theta a_{dr} + \left[(p+r)\cos\theta + re\right]a_{d\theta}\right) \tag{85b}$$

$$\frac{di}{dt} = \frac{r\cos u}{h}a_{dn} \tag{85c}$$

$$\frac{d\Omega}{dt} = \frac{r\sin u}{h\sin i}a_{dn} \tag{85d}$$

$$\frac{d\omega}{dt} = \frac{1}{he}\left[p\cos\theta a_{dr} + (p+r)\sin\theta a_{d\theta}\right] - \frac{r\sin u\cos i}{h\sin i} \tag{85e}$$

$$\frac{dM}{dt} = n - \frac{b}{ahe}\left[(p\cos\theta - 2re)a_{dr} - (p+r)\sin\theta a_{d\theta}\right] \tag{85f}$$

It can clearly be seen that the above equations are singular when either $e = 0$ or $i = 0$. The next appendix describes an alternative element set which eliminates these singularities.

B Non-Singular Elements

As shown in Appendix A, the Lagrange equations for the classical element set become singular when either e or i are 0. Physically, this may be interpreted as the effect of the line of nodes becoming indeterminate when $i = 0$ and the apsidal line disappearing when $i = 0$. In this appendix a non-singular element set eliminating these difficulties will be developed. The treatment given here is essentially that given by Battin **??**, it is included here for completeness.

The aim is to find variables that are combinations of the classical elements, and which are described by equations that are singularity free, for example if we introduce the mean anomaly,

$$l = M + \varpi \tag{86}$$

then when equations (85f) and (85e) are combined, we find

$$\begin{aligned}\frac{dl}{dt} = n - \frac{ae}{n(a+b)}[p\cos\theta a_{dr} - (p+r)\sin\theta a_{d\theta}] \\ -\frac{2br}{ah}a_{dr} + \frac{r\sin\theta\tan\frac{i}{2}}{h}a_{dr}\end{aligned} \tag{87}$$

which is free of singularites making l a suitable substitution for Mean Anomaly in the non-singular equation set. However inspection of equation[?] shows that it is dependent on true anomaly, θ which in turn is dependent on ω, a singular element. It will therefore be necessary to develop element substitutions that eliminate true anomaly from the equations. As a first step rewrite Kepler's equation for l

$$l = \varpi + M = \varpi + E = e\sin E \tag{88}$$

Define the eccentric longitude, K

$$K = \varpi + E \tag{89}$$

Kepler's equation then becomes

$$l = K + e\sin\varpi\cos K - e\cos\varpi\sin K \tag{90}$$

If we write the equation of the orbit in terms of true longitude L

$$L = \varpi + \theta \tag{91}$$

we have

$$r = \frac{p}{1 - e\cos\theta} = \frac{p}{1 + e\sin\varpi\sin L + e\cos\varpi\cos L} \tag{92}$$

Note that in both Kepler's equation, and the equation of the orbit that the terms $e\sin\varpi$ and $e\cos\varpi$ both appear, also observe that both of these terms are determinate for all values of e. These terms are therefore possible replacements for e and ϖ in the variational equations. To verify that these substitutions lead to non-singular equations, first define

$$P_1 = e\sin\varpi \qquad P_2 = e\cos\varpi \tag{93}$$

and obtain equations for these terms by differentiting with respect to time and substituting the already calculated values for $\dot{e}$ and $\dot{\varpi}$ to obtain

$$\frac{dP_1}{dt} = e\cos\varpi\frac{d\varpi}{dt} + \sin\varpi\frac{de}{dt} \tag{94}$$

These equations are non-singular, but contain terms in u the argument of latitude. We now attempt to find substitutions for u to complete the equation set. The true latitude may be written as

$$u = \omega + \theta \tag{95}$$

writing this equation in terms of true longitude, eliminates θ and ω from the equation

$$\theta = L - \Omega \tag{96}$$

Returning to the variational equation for P_1, substitute for $\sin\theta$

$$\sin\theta = \sin L\cos\Omega - \cos L\sin\Omega \tag{97}$$

to give

$$\begin{aligned}\frac{dP_1}{dt} &= -\frac{1}{h}[p\cos La_{dr} - (p+r)\sin La_{d\theta} - rP_1a_{d\theta}]\ldots \\ &\quad + \frac{r(\sin L\cos\Omega\tan\frac{i}{2} - \cos L\sin\Omega\tan\frac{i}{2}}{h}P_2a_{dn}\end{aligned} \tag{98}$$

Note in this equation that the combinations $\tan\frac{i}{2}\sin\Omega$ and $\tan\frac{i}{2}\cos\Omega$ appear, these terms are determinate for all values of i and possible non-singular replacements for i and Ω. Define the elements Q_1 and Q_2 as

$$Q_1 = \tan\frac{i}{2}\sin\Omega \qquad Q_2 = \tan\frac{i}{2}\cos\Omega \tag{99}$$

and derive the variational equations as before. For Q_1 obtain,

$$\frac{dQ_1}{dt} = \frac{r}{2h}(1 + Q_1^2 + Q_2^2)\sin La_{dn} \tag{100}$$

which is non-singular as required. The full set of equations are given in Section 2.

References

1. A. Lamy and S. Pascal. Station Keeping Strategies for Constellations of Satellites. In *AAS/AIAA Astrodynamics Specialist Conference 1993*, 1993. AAS 93-906.

2. David Leonard. Incredible Shrinking Spacecraft. *Aerospace America*, pages 21—24, January 1996.

3. A. E. Ballard. Rosette Constellations of Earth Satellites. *IEEE Transactions on Aerospace and Electronic Systems*, AES-16(5):656—673, September 1980.

4. J. G. Walker. Satellite Constellations. *Journal of the British Interplanetary Scoiety*, 37:559—571, 1984.

5. T. Foley. Big and Little LEOs face off. *Aerospace America*, pages 36—41, September 1995.

6. D. Smith and J. Hoot. Efficient Mission control for the 48 Satellite Globalstar Constellation. In *1st International Symposium on Reducing the cost of Space Ground Systems and Operations, Rutherford Appleton, Laboratory, Chilton, Oxfordshire, UK, 27-29th September, 1995*, 1995. RAL.GS.87.

7. P G Yarbrough. ORBCOMM Constellation Operations Approach. In *Proceedings IEEE Military Communications Conference MILCOM, 1995*, volume 2, 1995.

8. R. E. Glickman. TIDE:the Timed Destination Approach to Constellation Formation Keeping. In *AAS/AIAA Astrodynamics Specialist Conference 1994*, 1994. AAS 94-447.

9. C. R. McInnes. Autonomous Ring Formation for a Constellation of Satellites. Technical report, University of Glasgow, Department of Aerospace Engineering, 1994. Departmental Report 9624.

10. R. H. Battin. *An Introduction to the Methods and Mathematics of Astrodynamics*, chapter 10. AIAA Education Series. AIAA, New York, 1987.

11. D. King-Hele. *Satellite Orbits in an Atmosphere: Theory and Applications.* Blackie and Sons, Glasgow, 1987.

12. C. R. McInnes. Potential Function Methods for Autonomous Spacecraft Guidance and Control. In *AAS/AIAA Astrodynamics Specialist Conference, Halifax, Nova Scotia, 14-17 August,1995*, 1995.

13. C.R. McInnes and I. Lopez. Autonomous Rendezvous Using Artificial Potential Function Guidance. *Journal of Guidance, Control and Dynamics*, 18(2):237–241, March-April 1995.

14. C. R. McInnes and Frank McQuade. Co-Operative Control for the Fabrication of Extended Structures in Space. In *Proceedings of the AIAA/AAS Astrodynamics Specialist Conference, San Diego CA, Aug 1996.*, 1995.

15. C.R. McInnes. Large Angle Slew Manoeuvres with Autonomous Sun Vector Avoidance. *Journal of Guidance, Control and Dynamics*, 17(4):875–877, 1994.

16. M. Unwin. The PoSAT Microsatellite GPS Experiment. In *ION GPS-93, Salt Lake City, September, 1993*, 1993.

17. M. Unwin and M. Sweeting. A Practical Demonstration of Low-Cost Autonomous Orbit Determination using GPS. In *ION GPS-95, Palm Springs, September 1995*, 1995.